Article:

Abass, H. orcid.org/0009-0000-5693-0862, Goutianos, S., Qian, C. orcid.org/0000-0002-0414-7099 et al. (3 more authors) (2025) A failure mechanics study of aligned brick-and-mortar discontinuous long-fibre composites. Journal of Thermoplastic Composite Materials. ISSN 0892-7057

https://doi.org/10.1177/08927057251351555

Special Issue: Up to Editor if You Feel it Fits Well

JOURNAL OF THERMOPLASTIC COMPOSITE MATERIALS

A failure mechanics study of aligned brick-and-mortar discontinuous long-fibre composites

Journal of Thermoplastic Composite Materials
2025, Vol. 0(0) 1–31

Article reuse guidelines:
sagepub.com/journals-permissions
DOI: 10.1177/08927057251351555
journals.sagepub.com/home/jtc
Sage

Hussain Abass[1], Stergios Goutianos[2], Connie Qian[3], Paul Wilson[1], Neil Reynolds[1] and Ton Peijs[1]

Abstract

Aligned discontinuous long fibre (DLF) thermoplastic composites present a promising lightweight alternative to continuous fibre reinforced composites in high-volume applications. They offer a balance between mechanical properties and processability and provide an avenue for repurposing manufacturing waste. This study examines the mechanics of aligned DLF composites based on chopped discontinuous glass-fibre-reinforced polyamide-6 (PA6-GF60) unidirectional (UD) tapes as a function of tape length through a combined experimental and numerical simulation approach. Tensile tests, acoustic emission and 2D digital image correlation (DIC) were employed to investigate the stress-transfer and failure mechanics in aligned tape brick-and-mortar model composites, revealing critical stress-transfer lengths and initiation and propagation of various failure modes. A finite element analysis (FEA) damage model was developed to simulate the mechanical properties and stress-transfer mechanism in these composites, accounting for variability in tape properties and microstructures. The results revealed a transition from tape-tape interface failure to tape fracture as the dominant failure mode with increasing tape length, although even at higher tape lengths, failure was still initiated by tape pull-out in the skins. A critical tape length of approximately 15 mm was identified, beyond which mechanical properties no longer significantly improved. Results from both experimental and numerical methods showed good agreement, suggesting the model can be used to provide insights for property optimisation of these types of composites.

[1]WMG, University of Warwick, Coventry, UK
[2]Department of Manufacturing and Civil Engineering, NTNU, Trondheim, Norway
[3]School of Mechanical, Aerospace and Civil Engineering, University of Sheffield, Sheffield, UK

Corresponding author:
Hussain Abass, WMG, University of Warwick, Coventry CV4 7AL, UK.
Email: Hussain.Abass@warwick.ac.uk

Keywords

Discontinuous fibre composites, unidirectional tapes, thermoplastic composites, recycling, stress-transfer, fracture, mechanical properties, modelling, finite element analysis

Introduction

Aligned discontinuous long fibre (DLF) composites, also known as patched or arrayed chopped strand laminates, represent a specific class of discontinuous composites. These materials are manufactured by assembling discrete, aligned prepreg patches into laminates. They offer improved formability compared to continuous composites and are less prone to defects such as fibre wrinkling.[1] This characteristic makes them suitable for producing complex components, such as rib structures.[2] Furthermore, aligned DLF composites can be produced using prepreg waste generated during laminate manufacturing.[3] By cutting waste plies into the required tape dimensions, these offcuts can be repurposed and incorporated into a new laminate preform[4] using techniques including robot placement of offcuts[4] and mechanical alignment.[5]

As summarised in Figure 1, previous studies have demonstrated a trade-off between formability and mechanical properties when selecting discontinuous composites. DLF composites strike a balance between the high processability of short-fibre composites and the superior mechanical properties of continuous-fibre composites.[6,7] Through alignment, it is possible to increase the mechanical properties of DLFs above those of randomly oriented DLF composites.[8,9] This improvement approaches the mechanical performance

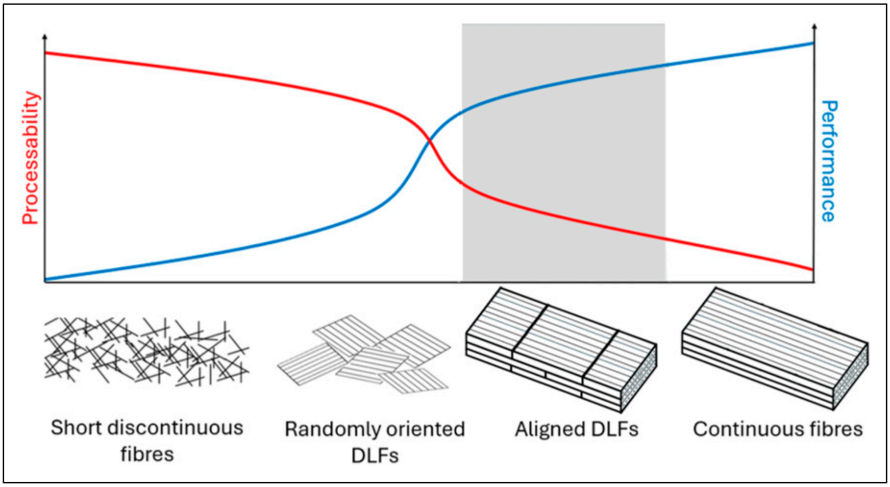

Figure 1. Processability and mechanical properties of various discontinuous fibre composite architectures. The gray shaded area represents the property and processability profile of aligned DLFs.

of continuous fibres when the DLFs have a sufficiently high aspect ratio, above which mechanical properties plateau.[10]

Using chopped UD tapes as reinforcing units, it is possible to produce composites with two levels of scale into a brick-and-mortar morphology, with reinforcing elements (tapes as bricks) bonded together with a thin layer of matrix (polymer as mortar). This morphology has been studied in several other composite systems which exhibit broadly the same mechanics (albeit at different length scales),[11] including the biological composite nacre (where hard aragonite tiles are embedded in a protein matrix),[12] arrayed 2D nanoparticles[13] and aligned discontinuous fibres.[14]

Stress transfer between individual tapes is a critical factor in the design of aligned DLF composites, as the interface between adjacent tapes is often the weakest point, where failure initiation and propagation are most likely to occur.[1] In addition to interface strength, stress transfer is significantly influenced by the overlap area between tapes[15] and matrix stiffness.[16] Given these sensitivities, modelling these composites effectively requires precise calibration of interface properties and a thorough understanding of the stress transfer mechanisms.

Various researchers have developed numerical simulation models for predicting the mechanical properties of DLF composites through the investigation of internal stresses. These have mostly included models of the mechanics of randomly oriented tape-based DLF composites. Earlier work implicitly represented each tape as an equivalent laminate, without modelling the interface interactions between the tapes.[17,18] Other authors modelled randomly oriented DLF composites with explicit representation of the tapes, such as Kravchenko et al.,[19] who modelled the tapes and interface using a 3D voxel mesh of randomly oriented platelets, while Ryatt et al. expanded on this study to accurately model stochastically oriented tapes while accounting for voids and waviness.[20,21]

Accurate models for aligned DLF composites are typically easier to develop than for randomly oriented DLF composites due to the reduced heterogeneity these composite systems have. The analytical shear-lag model by Pimenta et al.[22] accurately models the micro-mechanics in tension of brick-and-mortar DLF composites and has been applied to predict pseudo-ductile behaviour[23] and was later expanded to 3D geometries.[24] Meso-scale models of tape-based DLF composites have included the work of Shi et al.,[25] where tapes were assembled into designs with varying overlap lengths. In the work of Shi, the interface parameters were taken from material data sheets rather than estimated by fitting to experimental data such as digital image correlation (DIC) data. The latter approach was taken by Goutianos et al.[26] and Kussmaul et al.,[1] allowing more accurate predictions of performance at lower tape lengths (which are more dominated by interface properties). However, these authors did not account for the inherent variability in composite strength through stochastic determination of properties. In line with the theories of stochastic mechanics, such as the fibre break propagation model of Zweben and Rosen,[27] these variations in the material reduce the overall strength of the composite by creating a non-uniform stress field.[28,29] Therefore, there is a need for a modified modelling approach to evaluate the critical tape length in aligned DLF composites, such as characterising stress-transfer and interface parameters, and incorporating the stochastic failure characteristics of the reinforcing elements.

In addition to the challenges with capturing stress-transfer in numerical models, failure initiation and damage evolution in DLF composites are complex, necessitating full-field, in-situ monitoring to calibrate numerical models. DIC allows the tracking of local deformation in composites which can be used to characterise damage mechanisms.[18,30] X-ray computed tomography (CT) scans can be used for 3D analysis of composite failure modes *in-situ*[31] and combined with thresholding[32] or digital volume correlation (DVC) to track failure qualitatively.[33] Alternatively, in cases where failure is not visible (e.g. due to opaque specimens) and failure is multi-modal, previous works have used acoustic emission (AE) signals to identify failure mechanisms through correlating AE signals to particular failure events, for example through thresholding techniques,[34] correlating failure to the frequency of AE events[35,36] and unsupervised learning techniques.[37] This technique has been used to characterise failure in hybrid discontinuous-continuous fibre systems[34,38] and discontinuous fibre mats,[39] but to the best of our knowledge, has not been used to characterise the different failure modes of tape-based aligned DLF composites.

The mesoscale mechanics of aligned DLF composites have had little attention in the literature so far. Through FEA models, Kussmaul et al.[1] studied the optimal pattern for patched-aligned DLF composites while Shi et al.[25] studied the effect of different overlap lengths in different locations in the composite. However, these works lack an extensive experimental study of the underlying mesoscale mechanics which is necessary to validate these models at both the meso and macro scale. In addition, they do not incorporate the inherent stochastic properties of aligned DLF composites, such as variable tape strength.

In summary, there is a significant gap in the literature of experimental failure mechanics studies on aligned DLF composites. In addition, existing models lack both calibration with experimental results and incorporation of stochastic properties, reducing confidence in predictions. This gap is addressed in this study. The internal stresses and failure mechanics of aligned DLF composites based on chopped thermoplastic UD tapes were systematically studied using a variety of experiments and numerical simulations. The interfacial properties in aligned glass-fibre-reinforced polyamide-6 (PA6-GF60) tape-based composites were evaluated using the double-lap shear test. Damage initiation and propagation in the DLF composites were studied using AE, allowing the identification of different failure modes that occur for different mesostructures and tape lengths, as well as validating a stochastic FEA model. Alongside experiments, this was used to explore the mechanical properties of tape-based DLF composites as a function of tape length for a brick-and-mortar model composite. The FEA model was then used for the identification of the critical tape length, which is crucial for developing aligned DLF composites that exhibit an optimal balance between mechanical properties and processability.

Experimental methodologies

Specimen manufacturing

The material used was a continuous unidirectional (UD) tape of glass fibre-reinforced polyamide 6 (PA6) with 60 wt% (40 vol%) E-glass fibre (Celstran® CFR-TP PA6 GF60-03). Tapes were supplied by the Celanese Corporation and had an initial width of 305 mm, a thickness of 0.3 mm and an area density of 507 g/m^2. The melting temperature of the PA6 is 220°C.

Double-lap joint specimens. Double-lap joint specimens were manufactured to determine the interfacial properties between PA6-GF60 tapes. To investigate the effect of overlap length on mechanical properties, a double-lap joint of varying lengths was manually positioned between two discontinuous tapes of PA6-GF60 as shown in Figure 2. The overlap lengths used were 3 mm, 5 mm, 10 mm, 25 mm, 50 mm, 100 mm, and 150 mm. Given the difficulty of fusion bonding two thermoplastic materials, end tabs made from the same material were bonded to the ends of the tapes to prevent failure near the grips. Polytetrafluoroethylene (PTFE) films were placed either side of the single tapes to maintain the shape of the samples during the hot compaction processing but were removed before mechanical testing. Each sample was consolidated using the vacuum-bagging method (1 bar pressure) at 240°C for 12 min.

Brick-and-mortar specimens. Tensile specimens with an aligned "brick-and-mortar" structure were produced with nine plies. Continuous PA6-GF60 tapes were slitted as in Figure 3 to produce discontinuous tapes. Rectangular plaques of 300 mm × 300 mm x 3 mm were manufactured by laying up these cut plies into a perfectly aligned discontinuous "brick-and-mortar" mesostructure laminate. This resulted in butt joints between neighbouring tapes within the same ply, and an offset equal to $\frac{l_t}{2}$ was applied between

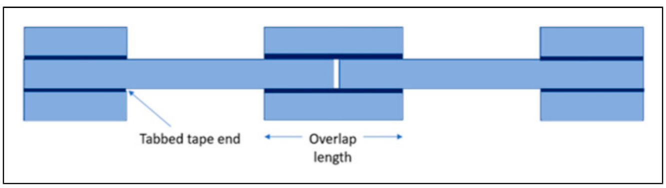

Figure 2. Tabbed double-lap joint specimen with overlap length indicated.

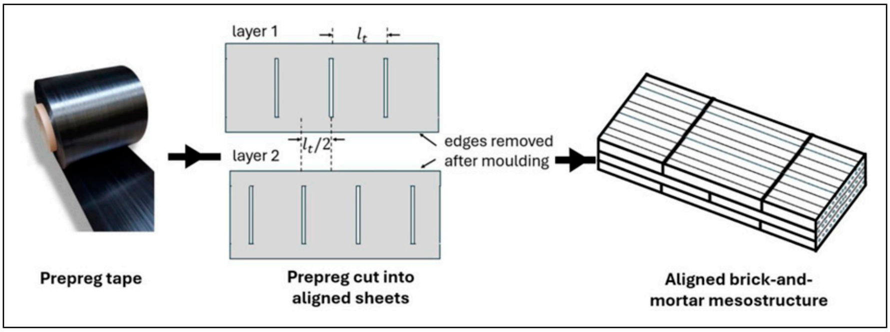

Figure 3. Schematic of the aligned DLF composites manufacturing route from cut UD tape and the resultant aligned "brick-and-mortar" mesostructure.

neighbouring plies, as shown for two plies (layers 1 and 2) in Figure 3. The resultant aligned regular brick-and-mortar mesostructure is also indicated in Figure 3. The chosen edge lengths l_t studied were 25 mm, 50 mm, 75 mm, 100 mm, 125 mm and 150 mm (constant tape size within each plaque) and were manufactured using the vacuum-bagging method (1 bar pressure) at 240°C for 16 min. Tensile specimens of 250 mm × 15 mm were cut from each plaque using a diamond cutting wheel in accordance with ASTM D638.

Due to inherent variability in the manufacturing process of the laminates due imprecise placement of discontinuities and placement of the layers in the brick-and-mortar structure, the location of discontinuities is accounted for by fitting the offset from a baseline location for several discontinuities to a normal distribution. Zeiss Xradia Versa 410 Micro-CT system with a voxel size of 10 μm, an accelerating voltage of 60 kV and a power of 15 W was used to image the specimens. The specimens were rotated 360° and 2879 projections with two frames per projection at 1050 sec exposure time and were collected on a charge-coupled device detector. An aluminium filter of 1 mm thickness and a source-detector distance (SSD) of 1200 mm were used. To obtain clear images, results from the μ-CT system were reconstructed using the Zeiss built-in reconstruction software and the scans were calibrated using a voxel scaling method.[40] 15 locations were measured and used to calculate a normal distribution which represents the probabilistic nature of the location of discontinuities. Examples of these discontinuities are shown in Figure 4. The parameters of the normal distribution were a standard deviation $\sigma = 2$ mm and a mean $\mu = 0$ mm.

Mechanical testing and DIC

Double-lap shear tests were performed using a Zwick Z250 testing machine at a cross-head speed of 1 mm/min. The specimen thickness was calculated as the average of the thickness at three points in the regions between the tab and overlap. Tensile tests on tape-based aligned DLF laminates were performed according to ASTM D638 with a gauge length of 150 mm and the specimen thickness was calculated by averaging the thickness at three points.

2D digital image correlation (DIC) technique was adopted for full-field strain measurements using the Zwick videoXtens biax-2-150 HP system. A white elastic spray paint was used to create a speckled pattern on the specimen. The images for 2D DIC analysis were captured using a camera resolution of 0.15 μm and a field of view of 103.9 mm × 69.4 mm with a sampling rate of 500 Hz.

Mechanical testing was also used to determine the properties of the UD tape. To determine tensile strength, 30 specimens of UD tape with a length of 250 mm were end-tabbed using the same method as for the double-lap shear specimens and were tested for tensile strength. Weibull statistical analysis was used to determine the Weibull modulus and characteristic strength, and to describe the size effect in the tape used in this study,[41] a valid approach at tape lengths significantly above the stress-transfer length as in this study. The Weibull modulus was calculated to be 18.96, and the characteristic strength was 824.1 MPa (see Appendix A). Tensile testing according to ASTM D3039 was used with varying laminate thicknesses to determine the remainder of the tensile properties using continuous UD tape for the 0° (5 plies) and 90° (10 plies) directions. The in-plane shear

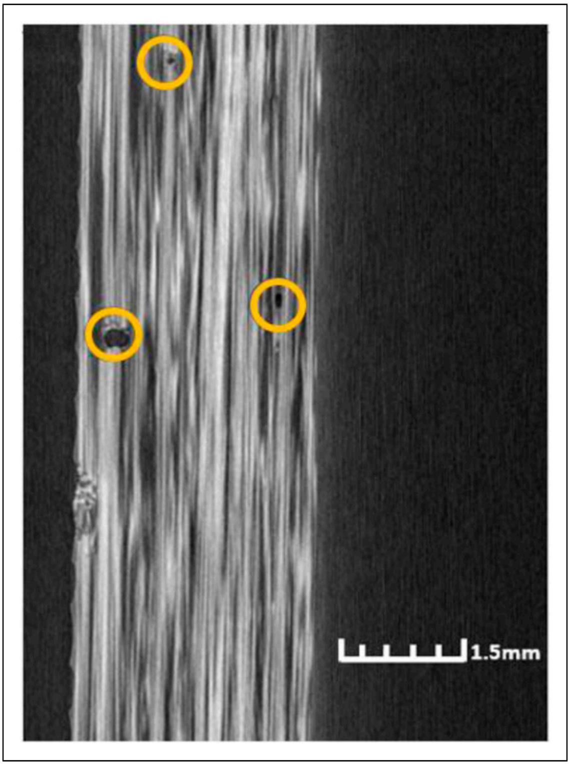

Figure 4. A μ-CT scan image of the aligned brick-and-mortar structure, showing that the discontinuities are offset from each other rather than aligned along the thickness. The yellow circles indicate discontinuities at tape ends.

properties were measured using static tensile testing on a ±45° laminate (16 plies) according to ASTM D3518 and assumed to be representative of the interlaminar shear properties.

Acoustic emission

AE analysis was performed using a Mistras PCI-2AE system with two wideband piezoelectric sensors (PICO-200-750 KHz, Mistras). The AE sensors were placed 100 mm apart on the specimen with silicon grease as an acoustic couplant between the sensor and the specimen surface. The signal was amplified using a Mistras In-line preamplifier with a gain of 26 dB. The threshold for the minimum strength of signals recorded was set to 45 dB and the sampling rate for acoustic data was set to 5 MHz. A Hsu-Nielsen pencil lead break test was used to calibrate the acoustic system for each specimen in accordance with ASTM Standard E976-94.

The main features of each acoustic event were extracted from the recorded acoustic signals using Fast Fourier Transformations (FFTs). A schematic summary of the definition of features for an AE signal is presented in Figure 5. Location sensing was used to account for the attenuation in the signal, since both the amplitude and energy of an acoustic wave would decrease as the distance from the source increases, following the general form:

$$B = B_0 e^{-\alpha x} \tag{1}$$

where B_0 is the amplitude or energy at the source location, x is the distance between the source and the sensor, and α is a constant specific to the measurement of amplitude or energy.

Two benchmark specimens were specifically designed, both consisting of nine UD plies with a single transverse slit or cut within each ply. The first specimen type had a very short overlap distance of 3 mm between the cuts in neighbouring plies, leading to pull-out only (Figure 6(a)). The second specimen had a very large offset distance of 150 mm between the cuts in neighbouring plies and long overlap lengths and was therefore expected to fail by tape and fibre fracture (Figure 6(b)).

Numerical simulation methodologies

FEA was used to estimate the performance of discontinuous aligned tape composites. While tape properties are assumed to remain constant, interfacial properties are less clearly defined and require an experimental study to be better understood. Given that the double-lap shear experiments may identify the transition from interface-dominated failure (tape pull-out) to fibre-dominated failure (tape fracture), these experiments were used as a benchmark to estimate the interfacial properties between UD tapes. While short tape-length aligned DLF composites are difficult to manufacture, modelling the interface failure using an estimated cohesive law allows for the assessment of composites with

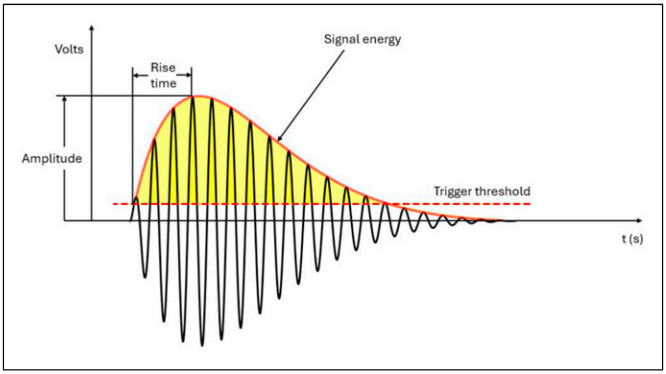

Figure 5. The parameters of an acoustic emission event.

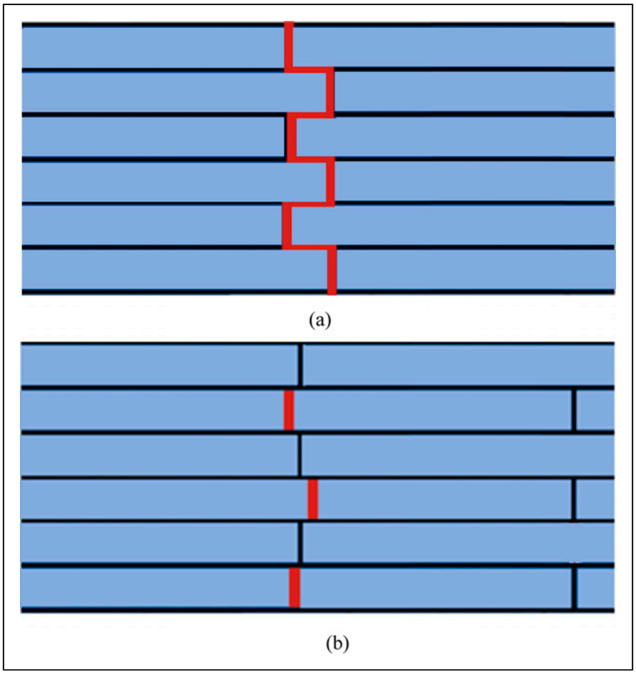

Figure 6. The two engineered mesostructures for AE analysis. The intended mode of failure is indicated in red. (a) Interlaminar shear failure with tape pull-out (short overlap length) and (b) tape failure with fibre breakage (long overlap length).

tapes shorter than the lowest experimentally tested length (25 mm) and the identification of a critical tape length. The aligned DLF composites are modelled with the stochastic discontinuity placement previously calculated.

FEA model parameters and setup

Tape model. The mechanical properties used in the model for the prepreg tape are given in Table 1. The tapes were modelled as a linear elastic material with elastic properties acquired from mechanical testing of UD tapes. Tape fracture initiation was modelled using the Hashin criteria with strength properties defined using the Weibull parameters,[42,43] while damage evolution was modelled using energy criteria using linear stiffness degradation. For each damage mode, the energy dissipated during the damage progression was set to 10 kJ/m^2.

Due to the strong non-linearities present in the model, convergence is difficult with an implicit FEA solver with a true static equilibrium. Therefore, an explicit FEA solver with mass scaling was used to overcome this under quasi-static conditions, and the tape material model was implemented using a user subroutine (VUMAT) in Abaqus. To minimise the dynamic effects of using the explicit solver, the sum of the kinetic energy was kept minimal to the internal energy dissipated (below 0.5% of the internal strain of the body), indicating the validity of assuming that the solution is quasi-static.[44] CPE4R plane strain elements were used for the tape. The individual tapes and interface regions were joined using tie constraints using the in-built Abaqus part merging feature.

Interface model. A matrix dominated region exists at the interface between the tapes in aligned DLF composites. Two main failure mechanism affect the interface in aligned DLF composites – matrix yielding and debonding. To model the plasticity of the matrix into their interface models, some authors have presented a range of possible values for the yield stress of the interface,[45,46] however, it is difficult to calibrate the elastic-plastic interface model without extensive experimental characterisation of the strain-field around cracks or with the stress-strain curve of the prepreg matrix. Instead, a common approach for simulating interfaces for DLF composites is used,[1,8,25,26,47] where the interface failure via both matrix yielding and debonding is captured entirely using an interface cohesive law, reducing the number of parameters needing tuning. This approach has been shown to effectively model the propagation of interlaminar failure under quasi-static loading.[48] The interfacial properties between PA6-GF60 tapes in the brick-and-mortar DLF composite

Table 1. Mechanical properties of the tape.

Material parameter	
Longitudinal modulus, E_{11}	35000 MPa
Transverse modulus, E_{22}, E_{33}	6800 MPa
Poisson's Ratio, ν_{12}, ν_{13}	0.36
Poisson's Ratio, ν_{23}	0.30
Shear modulus, G_{12}, G_{13}	2000 MPa
Shear modulus, G_{23}	1000 MPa
Longitudinal Weibull strength, X_{11}	824.1 MPa
Weibull modulus	18.96
Transverse tensile strength, Y_{22}	39 MPa
Longitudinal shear strength, S_{12}, S_{13}	22 MPa
Transverse shear strength, S_{23}	22 MPa

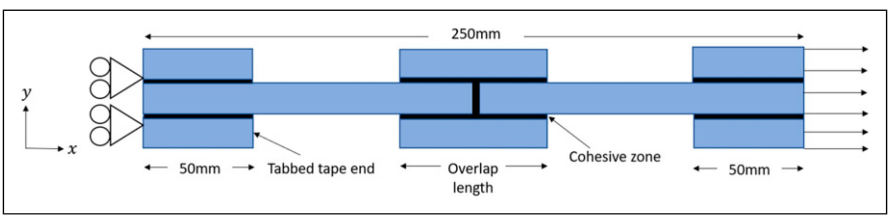

Figure 7. FEA model of the double lap shear test.

were determined by calibrating a 2D FEA model (Figure 7) of the double-lap shear tests against the experimental results. The model was constrained in the y-direction at one end of the specimen, and a displacement boundary condition in the x-direction was applied at the other end of the specimen with a smooth step function to avoid artificial inertia effects.[49] The interfacial behaviour between adjacent tapes was modelled with COH2D4 cohesive elements using a bilinear traction-separation law (Figure 8) defined by the maximum traction, fracture energy and interfacial stiffness. Other parameters of the cohesive law such as the gradients of the cohesive law and displacement at failure δ_n^f are calculated from these values.

For initial predications, mode I and mode II peak traction and fracture energy (approximately 45 MPa and 3 kJ/m^2 respectively[50,51]) traction-separation laws were assumed to be the same. The interface cohesive law was estimated by varying the fracture toughness of the FEA model while maintaining a constant interface strength and vice versa. These values were calibrated to experimental results, as detailed in Results and discussions - Stress transfer and debonding. The parameters used are shown in Table 2.

Modelling aligned DLF brick-and-mortar composites. The modelling of the aligned tape brick-and-mortar structure was performed similarly to the double-lap shear structure.

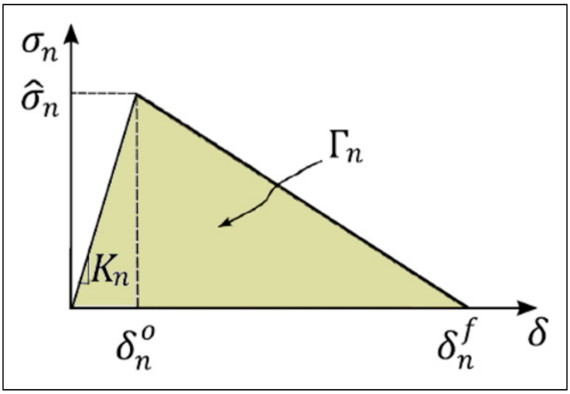

Figure 8. Bilinear interface cohesive law. The mode I interfacial traction energy is equal to the energy under the curve, K_n is the initial interface stiffness and the peak traction is $\hat{\sigma}_n$. Reproduced with permission from.[26]

Table 2. Interface mechanical properties.

Material parameter	
Young's modulus, E	2500 MPa
Shear modulus, G	1000 MPa
Peak traction, $\hat{\sigma}_n$	45 MPa
Fracture energy	3 kJ/m^2

Given that there is no variation in the orientation of the tapes in the manufacturing method in this study, a 2D FEA model with plane strain elements was assumed. The properties of the tape and interface in this model were the same as in the double-lap shear simulations, as are the parameters of the cohesive law and mesh parameters. The location of the discontinuities was introduced in line with the normal distribution calculated previously. Non-zero nodal displacements were applied to all nodes at one tape end, while nodes at the opposite tape end were constrained in the x-direction. The geometry of this model is shown in Figure 9. As shown in Figure 10 there is only a small impact of mesh refinement on the model. However, a 0.1 mm mesh refinement was used since computation speed was still acceptable and this ensured that for the smallest overlap length (3 mm) 30 cohesive elements were present at the interface.[52] At 0.1 mm refinement, the model ran on a local

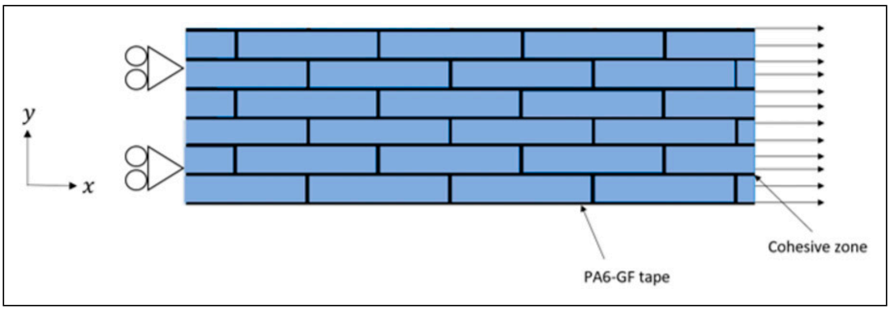

Figure 9. FEA model of the aligned brick-and-mortar specimens with a regular bond structure.

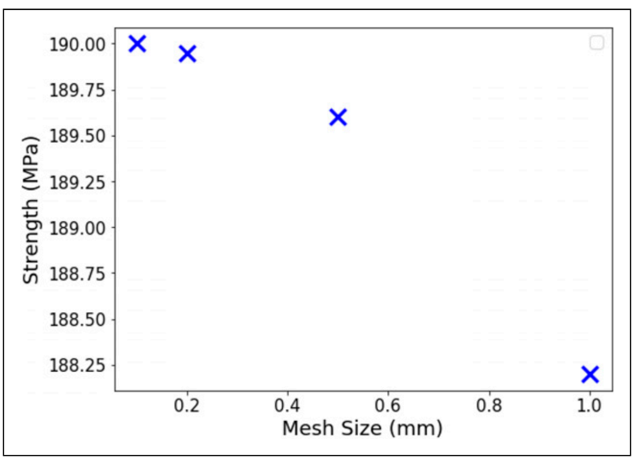

Figure 10. Mesh sensitivity study showing the impact of mesh refinement on the strength of a 5 mm overlap brick-and-mortar specimen. The values for approximate global size of the elements in the sensitivity study are plotted.

workstation equipped with Intel® Xeon® Gold 6128 processor (6 cores, 3.40 GHz) and 64 GB of RAM in 69 minutes.

Results and discussions

Stress transfer and debonding

Debonding. The evolution of failure stress in the double-lap shear samples based on experiments and FEA was studied as a function of the tape overlap length and is shown in Figure 11. This graph demonstrates the effect of overlap length on tensile strength, showing a sharp rise in strength up to 5-10 mm, after which the strength plateaus. This curve provides insight into the required minimum tape length for effective reinforcement, analogous to the well-known critical fibre length concept in composite micromechanics. The overlap length required to achieve around 50% reinforcing efficiency was approximately 3 mm. Given that the overlap length is twice the length of the overlap for each tape, the stress-transfer length reported is half the overlap length for 50% effective reinforcement, that is 1.5 mm. Additionally, the results indicate that the parameters of the traction separation law detailed in Table 2 (peak traction, $\widehat{\sigma}_n$ of 45 MPa and fracture energy of 3 kJ/m^2) provide a good fit to the experimental data.

The cracking mechanism can be identified by studying the mode mixity. The MMIXDMI parameter in Abaqus indicates the failure mechanism for all failed interface elements after complete failure in the simulation, with a value between 0 and 0.5 indicating Mode I failure and 0.5-1 indicating shear damage.[53] Figure 12 shows the value of the MMIXDMI parameter at the site of interface failure (adjacent to the discontinuity) at 3 mm overlap length. The results indicate that failure is heavily Mode II dominated. Stable crack growth initially occurs adjacent to the discontinuity and at the end of the overlap. Crack growth is pure Mode II adjacent to the discontinuity but mixed Mode I and Mode II at the ends of the overlap. Unstable crack growth occurs at specimen failure. At higher overlap lengths (e.g. 10 mm and above), failure does not occur at the discontinuity interfaces and failure instead initiates in the tape.

In Figure 11, the Mode I and Mode II parameters were assumed to be equal for the interface parameters. Figure 13 shows the sensitivity to varying the properties of Mode I interface (increasing $\widehat{\sigma}_n$ by a factor of two and decreasing it by a factor of 10), showing little impact on properties. This further indicates the dominance of Mode II on failure and indicates that assuming Mode I properties are equal to Mode II is a reasonable assumption.

The crack propagation at the interfaces of short tape (e.g. 3 mm) aligned brick-and-mortsr DLF composites undergoes a stable Mode II dominated crack propagation in the range of approximately 0.3-0.7 mm, followed by unstable pure Mode II crack propagation at maximum load, similar to the double overlap specimens. At longer tape lengths (e.g. >10 mm), only stable crack propagation occurs, in the range of 0.3-1.2 mm, with failure dominated by tape failure. Given that crack propagation is over small distances, it is likely that this governs mesh convergence.

Stress transfer. For qualitative evaluation, the in-plane stress transfer is imaged in Figure 14 by plotting shear strains using DIC. This demonstrates the presence of stress

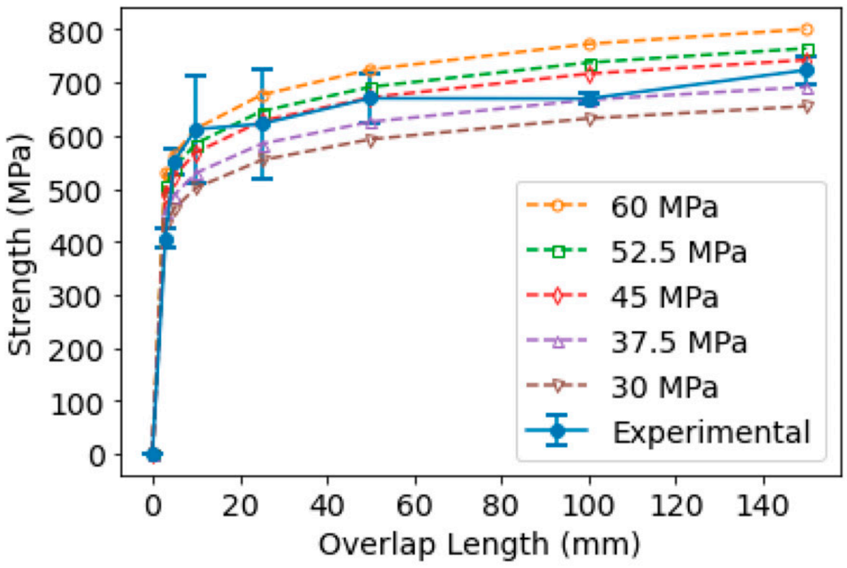

(a)

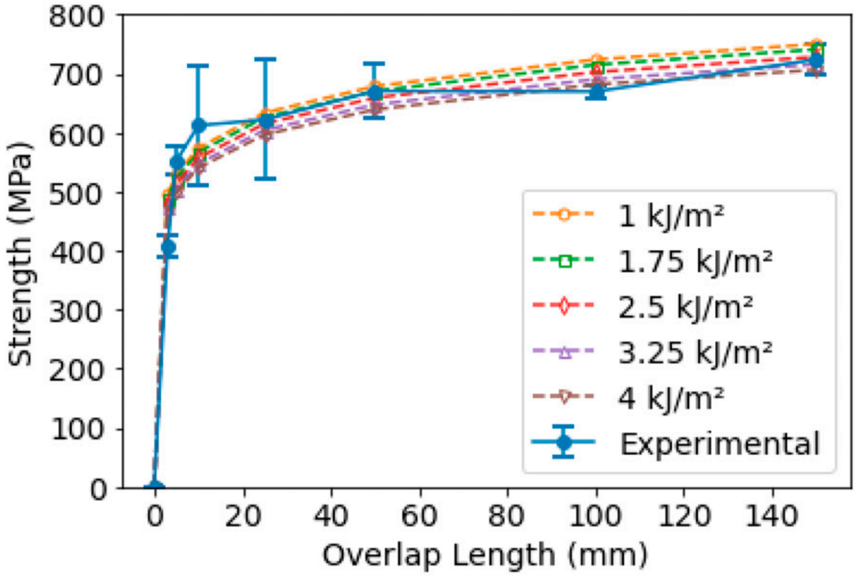

(b)

Figure 11. The effect of varying (a) peak traction (with fracture energy of 3 kJ/m^2) and (b) fracture energy (with peak traction, $\widehat{\sigma}_n$ of 45 MPa) in the cohesive zone model on FEA tensile strength predictions together with experimental data for the double-lap joint tensile tests.

concentrations at the discontinuity and shows a characteristic 'H-shape' through the variation of positive and negative shear strains. In Figure 15, the axial strain profile across a discontinuity is shown for a brick-and-mortar specimen of 125 mm tape length just before ultimate failure. The axial strain was plotted along the section across the discontinuity. Given that the spatial resolution allows the computation of strains within the stress transfer region, there is confidence that both the stress transfer length and shape are representative of the mechanics. Figure 15 shows the axial strain in the neighbouring tapes near a discontinuity. Its shape resembles that of a strain concentration arising from a fibre break in a unidirectional composite.[54] The DIC study also indicates that the chosen

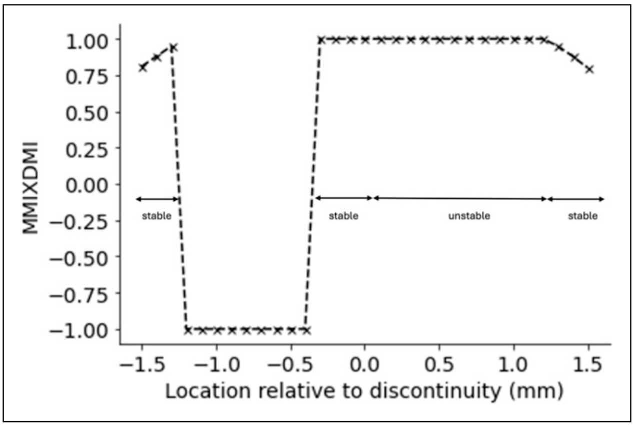

Figure 12. The mode mixity parameter MMIXDMI plotted along the interface for the 3 mm overlap length. A value of −1 indicates no failure, 0 is for pure Mode I failure and 1 is pure Mode II failure. The stability of the crack by location is also indicated.

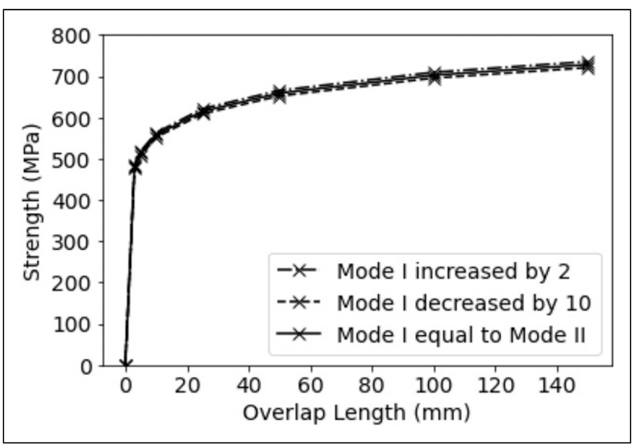

Figure 13. The effect of varying Mode I traction on properties at each overlap length.

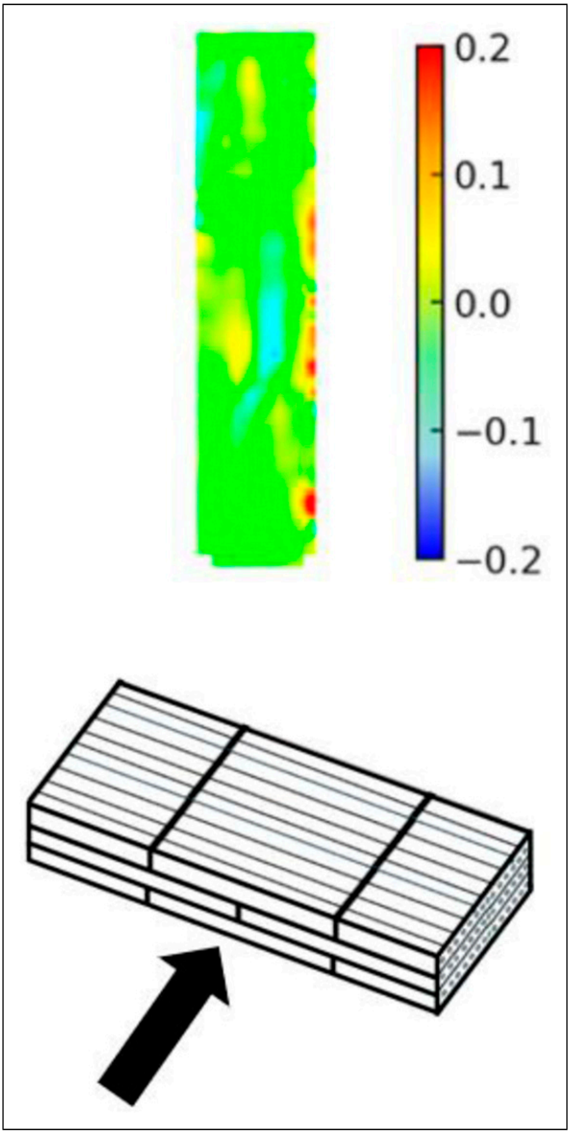

Figure 14. The shear strain distribution for a 125 mm brick-and-mortar specimen imaged from the side with DIC.

interface stiffness of 2.5 GPa provided a good fit of the experimental stress-transfer data (see Figure 15). An approximate stress-transfer length of 1-1.5 mm is observed, corresponding to a critical fibre length l_c of 2-3 mm. This is similar to the analytical result for l_c based on the elastic-perfectly plastic Kelly-Tyson model, where l_c for a platelet system is obtained as follows:

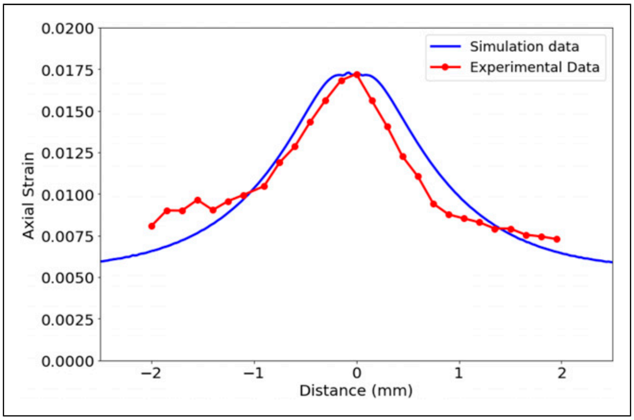

Figure 15. Axial strain by DIC and FEA versus distance from a tape discontinuity in the fibre direction.

$$l_c = \frac{\sigma_f d}{2\tau} \tag{2}$$

where d represents the reinforcement diameter, τ is the interface shear strength and σ_f is the reinforcement strength at l_c.[55] For values $\tau = 45$ MPa, $\sigma_f = 824.1$ MPa and $d = 0.3$ mm, $l_c = 2.75$ mm, showing general agreement between the experimental and FEA results and the model.

Acoustic emission failure analysis

Since failure in composites is typically multimodal, correlating each signal to a failure mechanism is a complex process.[34,56–58] To address this, the model specimens with biased failure modes where one mode dominates were used to correlate signal features with each failure mode using the energy and amplitude of signals, as in the work of de Groot et al.[59] and Fotouhi et al.[23] Fibre fracture and tape-tape interface failure are the most critical failure modes in tape-based DLF composite specimens subjected to in-plane tensile loads,[17] and the SEM images of failed interface and fibre fracture specimens are shown in Figure 16.

The amplitudes of AE signals obtained from the specimen that failed by either tape fracture or tape-tape interface failure are shown in Figure 17. The initiation of damage was taken to be the first significant increase in cumulative AE energy. The negligible value of cumulative energy at low strains for the 150 mm overlap specimen, indicates that damage was initiated at just over 1% strain, that is at around 92% of the ultimate failure strain, as shown in Figure 17(a). This contrasts with Figure 17(b), showing the variation of AE amplitude and cumulative energy for the interface failure dominated specimen. Here damage initiated at 0.54% strain, that is, at 68% of the ultimate failure strain. Between damage initiation and final failure, the detected AE events displayed amplitudes ranging from 60 dB to 75 dB.

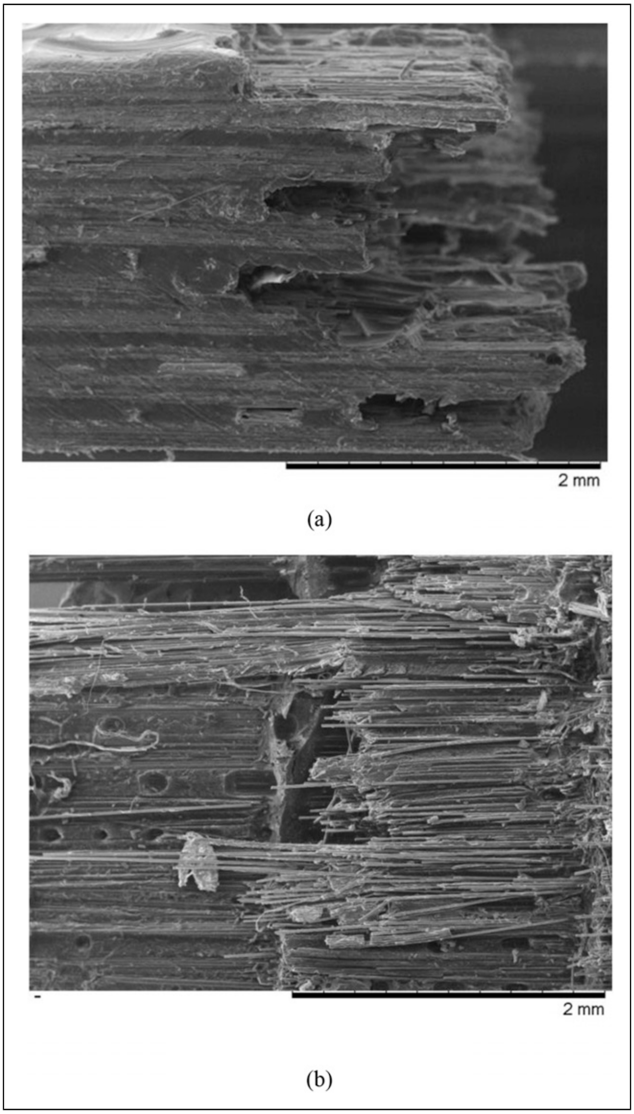

Figure 16. SEM images (×50 magnification) of the failure site for (a) a 3 mm overlap laminate, with tape pull-out after interface failure evidently the dominant failure mode (b) a 150 mm overlap laminate, where significant fibre failure is observed.

For both specimens, prior to damage initiation, AE signals were dominated by low amplitudes (<60 dB) and energy signals and were therefore considered background noise. To test the origins of these noise signals, a mechanical test was performed on a neat PA6 tensile specimen which did not result in any detected hits above the 45 dB threshold.

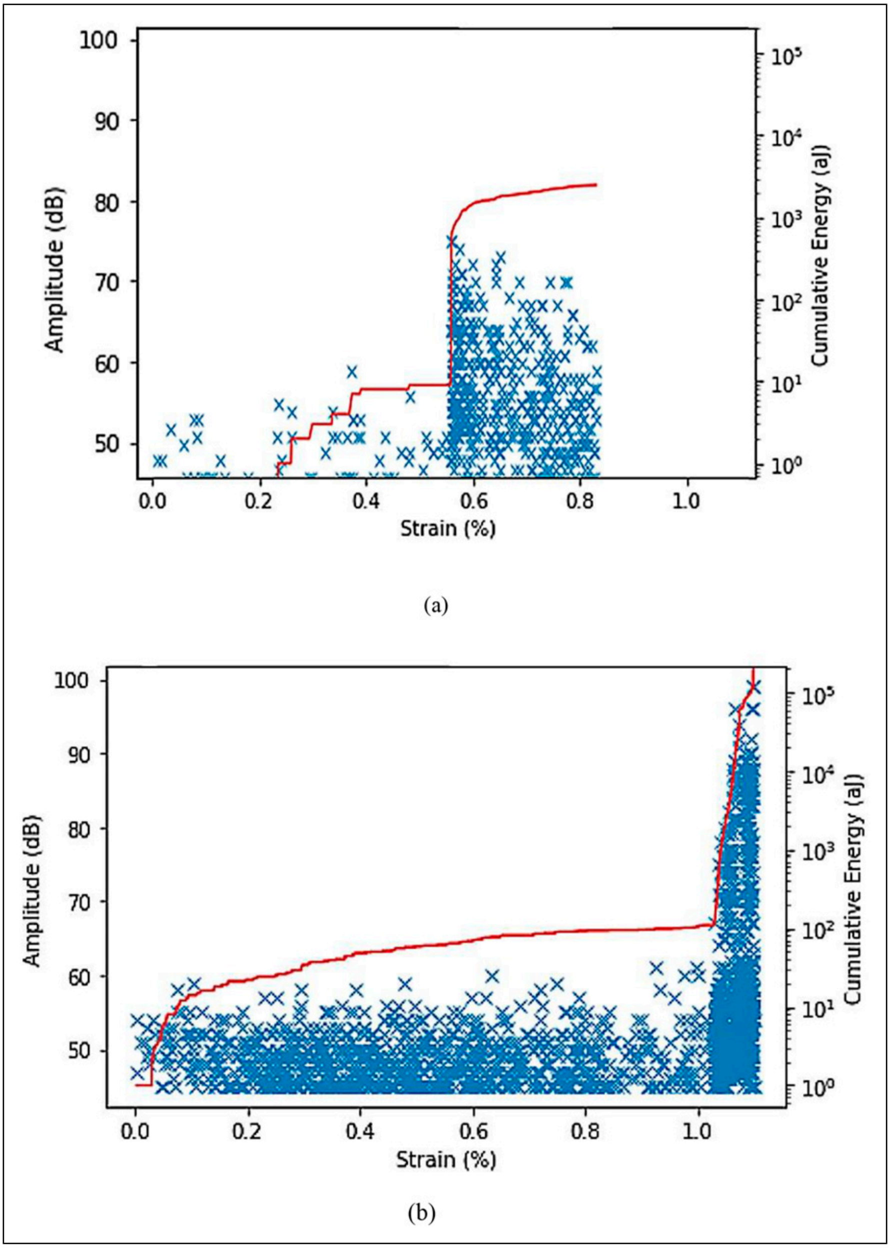

Figure 17. Plots of amplitude of AE events and corresponding cumulative energy in (a) a specimen with a 3 mm overlap length between tapes and interface failure followed by tape pull-out as the dominant failure mode and (b) a specimen with a 150 mm overlap length between tapes and tape fracture as the dominant failure mode.

In the case of ductile plastics like PA6, AE events are not likely to occur due to matrix yielding (in contrast to brittle epoxy matrices, where matrix cracking events are reported to exceed this threshold amplitude[60]). Comparing the AE data for these specimens indicates that high-energy and high-amplitude events are characteristic of fibre breakage, as these events occur exclusively in the 150 mm overlap specimen. Additionally, since failure in the 3 mm overlap specimen was dominated by interface failure, it can be concluded that hits in the range 60 to 80 dB are related to interface failure, since these events occur after damage initiation, and mid-range hits are attributed to delamination and debonding.[57] To analyse the initiation and propagation of each damage mode separately,

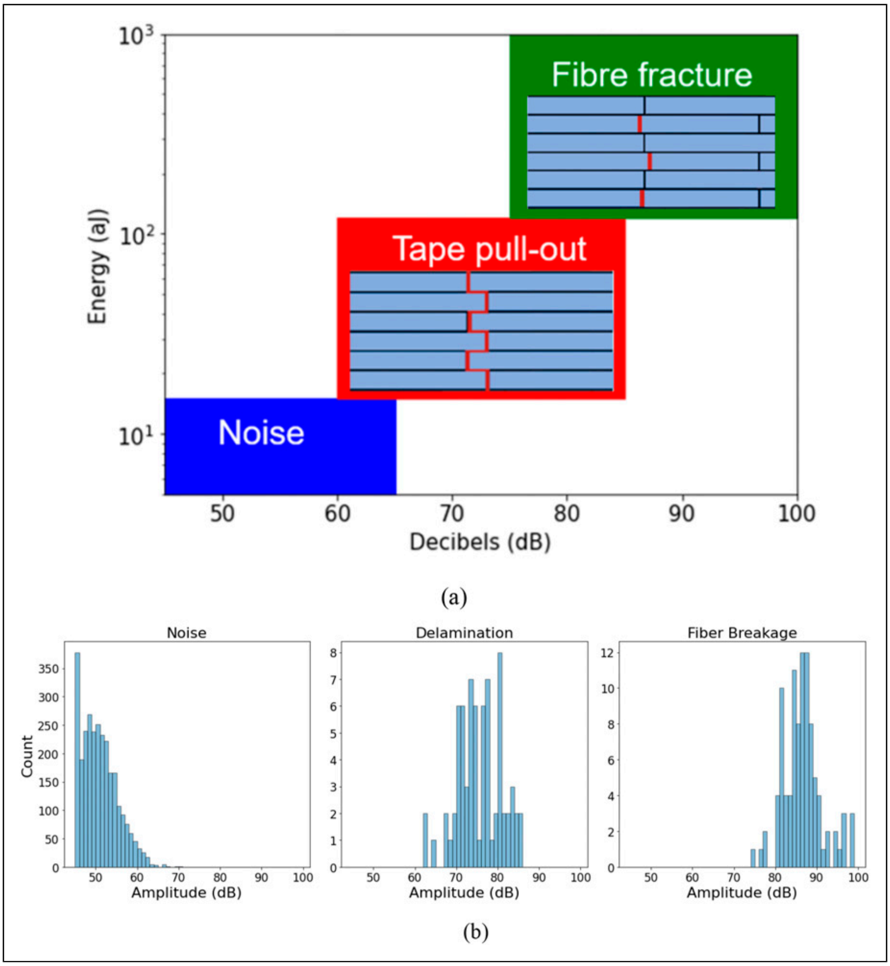

Figure 18. (a) The amplitude and energy of events as assigned to the different failure modes. (b) Counts of AE events by amplitude for the energy range associated with each failure mode for a 150 mm overlap brick-and-mortar specimen.

the failure modes were mapped to the corresponding energy and amplitude of their events, as shown in Figure 18(a). The distribution of amplitudes for each energy range for a typical 150 mm overlap specimen is indicated in Figure 18(b), which shows that while there are overlaps in data ranges, these are of a negligible value. The three ranges are (1) signals attributed to background noise, with 0-15 aJ energy and 45 to 65 dB amplitude, (2) signals attributed to interface failure with 15-120 aJ energy and 60 to 85 dB amplitude and (3) signals attributed to tape and fibre fracture with energies greater than 120 aJ and amplitudes greater than 75 dB.

The classification results are used to describe the initiation and propagation of each failure mode in the 150 mm overlap specimen by plotting the energy progression of each mode of failure. Since failure is solely due to interface failure in the 3 mm overlap specimens, this is not repeated for these specimens. As shown in Figure 19, the first significant AE events are related to interface failure. This failure mode initiated at 92% ultimate strain, or 1.02% strain. Fibre fracture initiated at 95% ultimate strain, corresponding to 1.05% strain. Most of the energy dissipated in the failure of the sample was from fibre fracture, as shown by tracking the final positions of the cumulative energy curves.

A direct comparison of the number of AE events in each specimen is presented in Figure 20. The larger number of AE events for the 150 mm overlap specimen is clearly due to the much larger number of failure sites (fibres) compared to the fewer failure sites in the 3 mm overlap specimen, where damage occurs at the tape-tape interface. Similar results have been found by other authors, for example Barkoula et al.,[61] who similarly

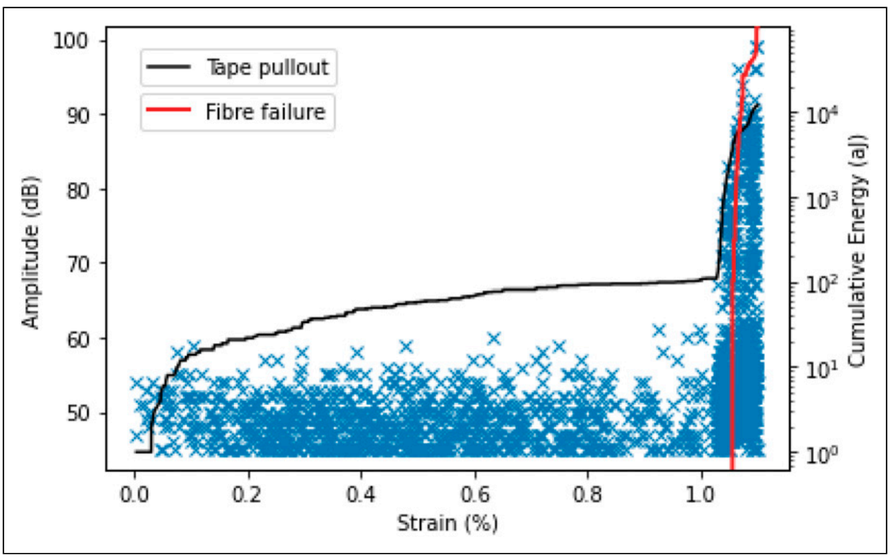

Figure 19. The cumulative energy of each failure mode for the 150 mm overlap aligned-DLF specimen.

reported a higher number of AE events for composites with fibre-dominated failure modes compared to composites with tape-dominated failure modes.[61]

Figure 21 shows a comparison between numerical simulations and experimental data, together with the corresponding damage initiation point determined by AE. The stress-strain curves indicate a relatively accurate prediction of the strength and stiffness of the composites. The order of failure mode initiation for the 150 mm specimen is accurately described, with failure initiating by interface failure at 94% of ultimate strain shortly before fibre breakage initiates at 97% of ultimate strain. The close correlation between

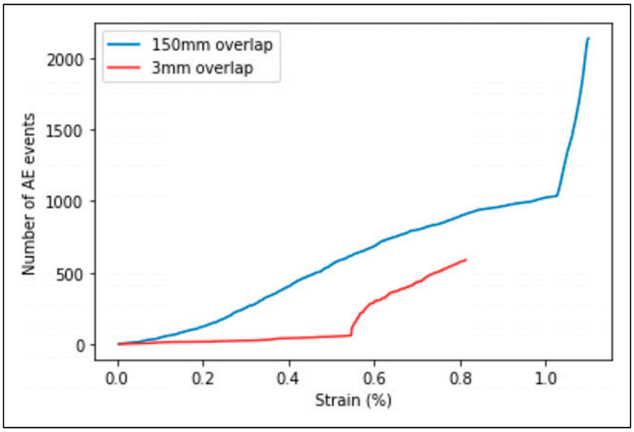

Figure 20. Cumulative count of AE events with varying strain for each specimen.

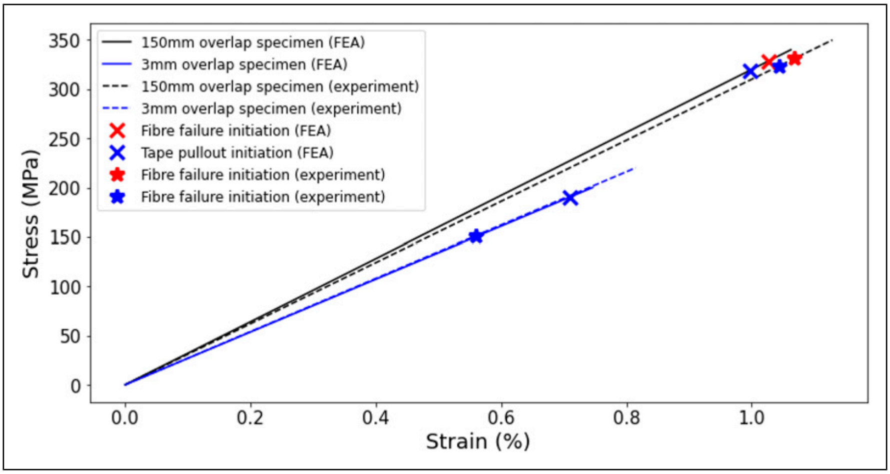

Figure 21. The initiation of interface failure and fibre fracture for the two specimens according to simulation and as detected by AE monitoring.

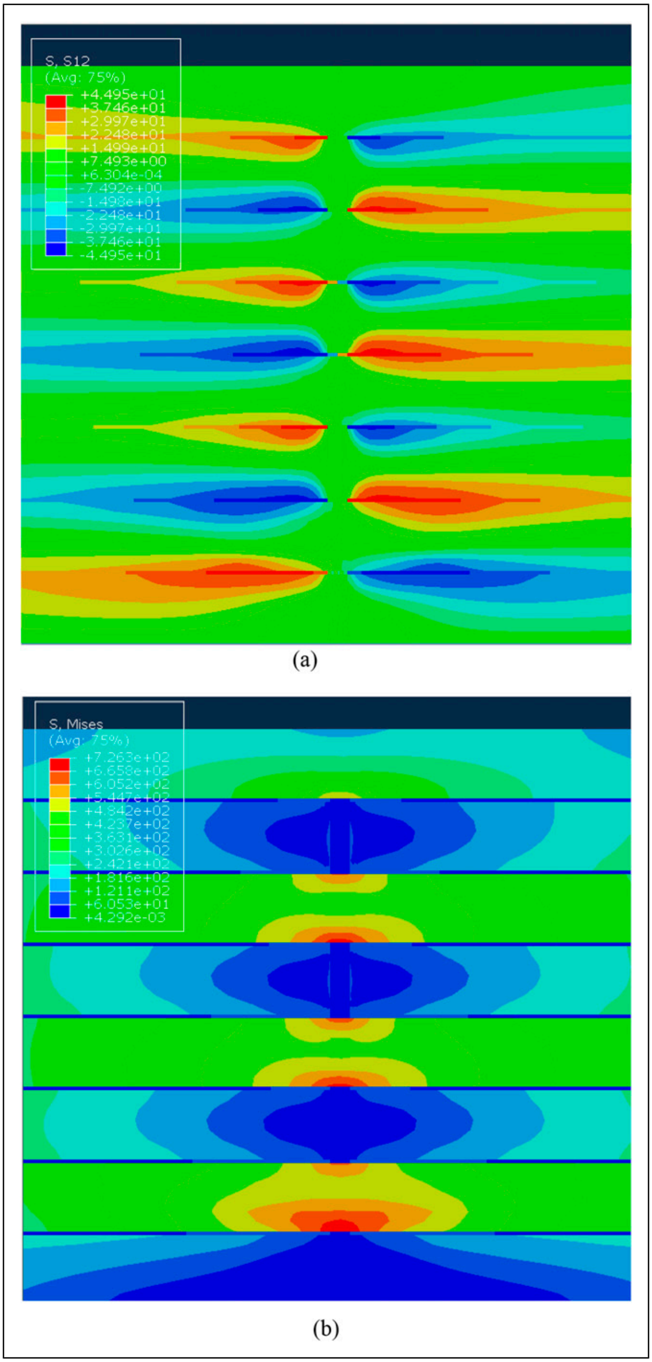

Figure 22. (a) The distribution of shear stress (MPa) through the thickness of a specimen before failure initiation. (b) The distribution of von Mises stress (MPa) through the thickness of a specimen before failure initiation.

failure mode initiations indicates the accuracy of the tuning performed in this work. As shown in Figure 22(a), according to the simulation, tape-tape interface failure initiates in the outer skins of the composite. This can be expected as tapes on either side of a discontinuity in the skin can only be loaded from one side of the tape, facing the core region. Hence, the shear stress at the interface of a tape in the skin must theoretically be double the shear stress at the tape-tape interface in the core to load the tape to the same tensile stress. This results in a higher shear stress and early failure of the interface for tapes in the skins than the core. It is further noted that fibre breakage initiates at a location adjacent to the initiation of interface failure, as indicated in Figure 22(b), where a clear stress concentration is observed next to the location of interface failure initiation. It is noted that the simulations in Figure 22 used an exact brick-and-mortar geometry with no stochastic offset or stochastic tape strength to avoid stochastic effects on mechanics.

The results for the 3 mm specimen indicate that the initiation of interface failure according to simulation was significantly later than in the experimental results. There could be several reasons for this discrepancy, including the inadequacy of the traction-separation law to describe interface failure, the necessity of defining a different criterion for damage initiation using AE or variability in the interface strength resulting in earlier local failures.[62] In this study, damage onset was described as the first significant increase in cumulative energy (which is inevitably the first significant failure event), however, this may not correspond to the initiation of interface failure and failure initiation may be better described by surpassing a certain proportion of energy. This would explain the relatively accurate prediction of failure initiation for the 150 mm specimen, since the cumulative energy curve in Figure 19 has a high gradient, indicating rapid propagation of damage. However, the rate of cumulative energy for the 3 mm specimen in Figure 17(a) was highest at the onset of damage, which may indicate that another method is needed to accurately describe the cumulative energy threshold for damage onset.

Effect of tape length on mechanical properties

Figure 23(a) shows the FEA predictions for three simulations alongside experimental results for the tensile strength of aligned brick-and-mortar DLF composites as a function of tape length. The results show that the experimental results were accurately modelled by the FEA model. Due to the difficulties of manufacturing brick-and-mortar samples at short tape lengths (<10 mm), these are modelled using the FEA model. As expected, at very small overlap lengths (<4 mm), the FEA model predicts failure to be dominated by cohesive (interface) failure, while at higher tape lengths, both experimental and FEA studies demonstrate that failure is dominated by tape (read:fibre) fracture. This is in line with the results of the double-lap shear experiments, which demonstrate that the critical stress transfer length is approximately 2 mm. The FEA model indicates that 90% of the plateau strength is reached with a tape length of approximately 15 mm. Similar results are observed for the effect of tape length on stiffness as shown in Figure 23(b), albeit at lower tape lengths (∼10 mm). This again agrees with micromechanical models for short fibre composites, which typically predict an earlier plateau for modulus than strength with

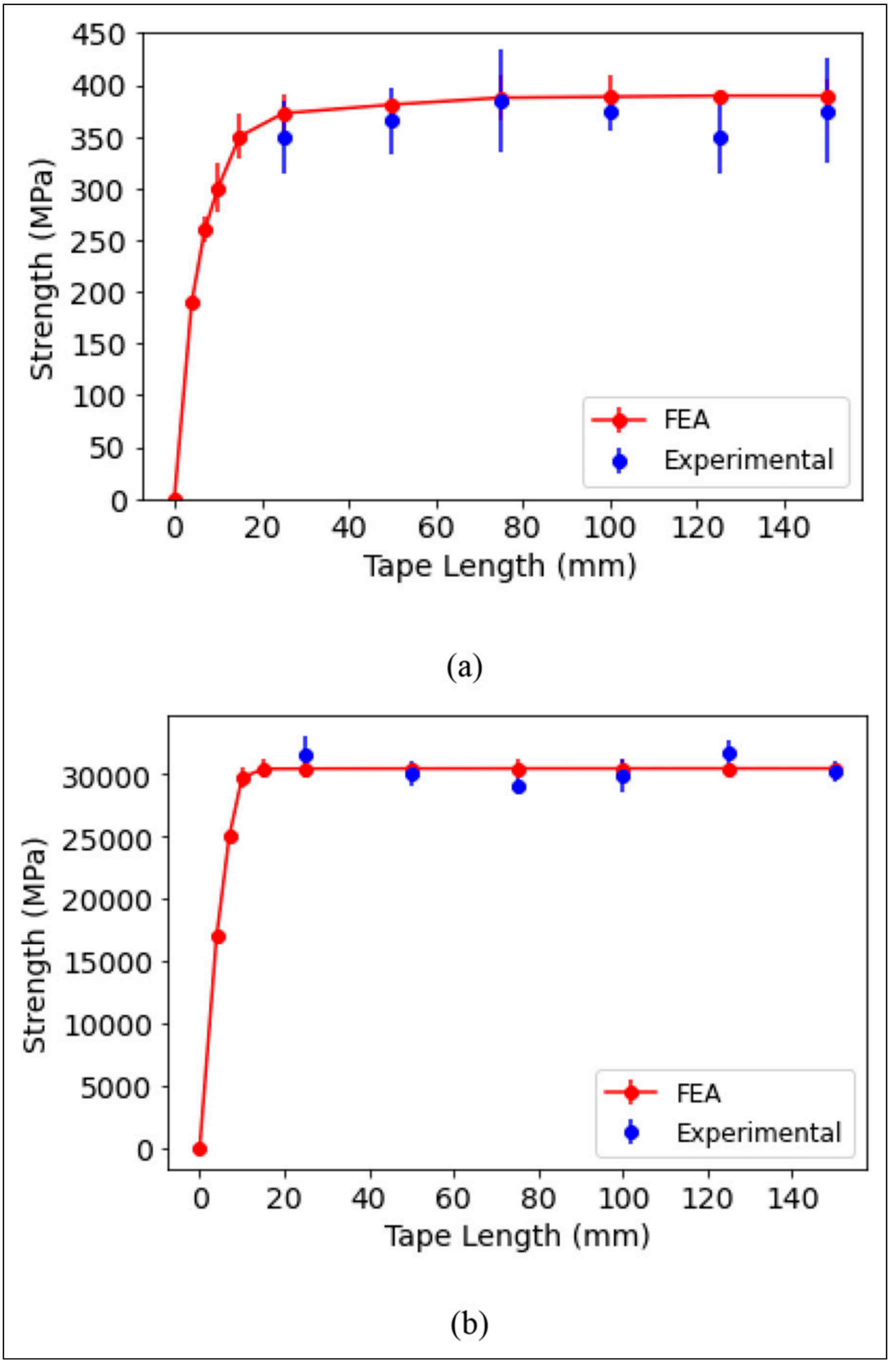

Figure 23. Influence of tape length on (a) tensile strength and (b) Young's modulus of aligned brick-and-mortar DLF composites; FEA simulations versus experimental data.

increasing fibre length.[63] The plateau strength is approximately 50% of the tape strength, which is expected given that for a regular-bond brick-and-mortar structure, tape ends are aligned, meaning the volume fraction is half that of the tape in the tape end area.

Conclusions

In this work, the mechanics of aligned DLF thermoplastics composites were characterised using idealised model experiments and FEA simulations. Double-lap shear experiments were used to investigate the dominant failure mode for composites with variable tape lengths. Given that the double-lap shear joint is representative of the joints in aligned tape-based DLF composites with brick-and-mortar architectures, this test provides real insight into the failure mechanism of these structures. DIC was used to characterise the stress transfer across a tape-end discontinuity, revealing a characteristic ‘H-shape’ profile when viewed in plane. AE signals were correlated to tape-tape interface failure and fibre-dominated tape fracture and used to identify the progression of different failure mechanisms at different tape lengths. A stochastic FEA model was developed based on these experiments showing a good correlation with experimental results for meso and macro level stress-strain response together with the propagation of fibre fracture in the tapes. The key results can be summarised as follows:

- A transition from the dominant failure mode of interface failure to fibre-dominated tape fracture is observed with increasing tape length for aligned DLFs, with the critical tape length for this change in failure mode leading to a plateau in properties being approximately 15 mm. At this critical tape length, the mechanical properties of the aligned DLFs reach a plateau at 50% of UD tape strength due to the use of a regular bond structure
- At higher tape lengths, failure also initiates by tape-tape interface failure but is closely followed by fibre-dominated tape fracture, which then becomes the dominant failure mode.
- FEA indicates that failure is primarily initiated by tape-tape interface failure in the outer skins of the laminate. This occurs because tapes located in the outer skins have only half of the interfacial area available for stress transfer, in contrast to tapes situated near the core.

The developed FEA model accurately captures the mesoscale mechanics of aligned DLF composites. It can therefore be used for the design and optimisation of composite mesostructures and to assess the impact of variability and manufacturing defects on mechanical performance. Further work on the influence of such defects and variability in the location of tape end discontinuities is currently underway together with an optimisation framework to maximize mechanical properties.

Acknowledgements

Funding for this project from the EPSRC under grant EP/T51794X/1 is acknowledged. The X-ray computed tomography (XCT) data used in this article was acquired using the Free-at-Point-of-Access scheme at the National Facility for X-Ray Computed Tomography (NXCT) and carried out at the Centre for Imaging, Metrology, and Additive Technologies (CiMAT) at the University of Warwick under the EPRSC Project Number (EP/T02593X/1).

Declaration of conflicting interests

The authors declared no potential conflicts of interest with respect to the research, authorship, and/or publication of this article.

Funding

The authors disclosed receipt of the following financial support for the research, authorship, and/or publication of this article: This work was supported by the EPSRC (EP/T51794X/1).

ORCID iD

Hussain Abass https://orcid.org/0009-0000-5693-0862

References

1. Kussmaul R, Zogg M and Ermanni P. A failure mechanics and strength optimization study for patched laminates. *Compos Struct* 2019; 226: 111165.
2. Taketa I, Okabe T and Kitano A. A new compression-molding approach using unidirectionally arrayed chopped strands. *Compos Part A Appl Sci Manuf* 2008; 39: 1884–1890.
3. Nilakantan G and Nutt S. Reuse and upcycling of thermoset prepreg scrap: case study with out-of-autoclave carbon fiber/epoxy prepreg. *J Compos Mater* 2018; 52: 341–360.
4. Gardiner G. Cevotec extends Fiber Patch Placement to sandwich structures, large aero-structures and enables combining with AFP. *Composites World*. 2018. https://www.compositesworld.com/news/cevotec-extends-fiber-patch-placement-to-sandwich-structures-large-aerostructures-and-enables-combining-with-afp.
5. Gillet A, Mantaux O and Cazaurang G. Characterization of composite materials made from discontinuous carbon fibres within the framework of composite recycling. *Compos Part A Appl Sci Manuf* 2015; 75: 89–95.
6. Visweswaraiah SB, Lessard L and Hubert P. Tensile behaviour of hybrid fibre architectures of randomly oriented strands combined with laminate groups. *J Compos Mater* 2019; 53: 3725–3740.
7. Selezneva M and Lessard L. Characterization of mechanical properties of randomly oriented strand thermoplastic composites. *J Compos Mater* 2016; 50: 2833–2851.
8. Sommer DE, Kravchenko SG, Denos BR, et al. Integrative analysis for prediction of process-induced, orientation-dependent tensile properties in a stochastic prepreg platelet molded composite. *Compos Part A Appl Sci Manuf* 2020; 130: 105759.
9. Feraboli P, Peitso E, Deleo F, et al. Characterization of prepreg-based discontinuous carbon fiber/epoxy systems. *J Reinforc Plast Compos* 2009; 28: 1191–1214.

10. Kratmann KK, Sutcliffe MPF, Lilleheden LT, et al. A novel image analysis procedure for measuring fibre misalignment in unidirectional fibre composites. *Compos Sci Technol* 2009; 69: 228–238.
11. Begley MR, Philips NR, Compton BG, et al. Micromechanical models to guide the development of synthetic "brick and mortar" composites. *J Mech Phys Solids* 2012; 60: 1545–1560.
12. Narducci F and Pinho ST. Exploiting nacre-inspired crack deflection mechanisms in CFRP via micro-structural design. *Compos Sci Technol* 2017; 153: 178–189.
13. Cilento F, Martone A and Giordano M. Insights on shear transfer efficiency in "brick-and-mortar" composites made of 2D carbon nanoparticles. *Nanomaterials (Basel)* 2022; 12: 1359.
14. Henry J and Pimenta S. Modelling hybrid effects on the stiffness of aligned discontinuous composites with hybrid fibre-types. *Compos Sci Technol* 2017; 152: 275–289.
15. Mendels DA, Leterrier Y and Manson JAE. Stress transfer model for single fibre and platelet composites. *J Compos Mater* 1999; 33: 1525–1543.
16. Yu Y, Zhang B, Tang Z, et al. Stress transfer analysis of unidirectional composites with randomly distributed fibers using finite element method. *Compos B Eng* 2015; 69: 278–285.
17. Selezneva M, Roy S, Lessard L, et al. Analytical model for prediction of strength and fracture paths characteristic to randomly oriented strand (ROS) composites. *Compos B Eng* 2016; 96: 103–111.
18. Feraboli P, Cleveland T, Stickler P, et al. Stochastic laminate analogy for simulating the variability in modulus of discontinuous composite materials. *Compos Part A Appl Sci Manuf* 2010; 41: 557–570.
19. Kravchenko SG, Sommer DE, Denos BR, et al. Tensile properties of a stochastic prepreg platelet molded composite. *Compos Part A Appl Sci Manuf* 2019; 124: 105507.
20. Ryatt J and Ramulu M. Prediction of tensile failure of stochastic tow-based discontinuous composites via mesoscale finite element analysis. *Compos Struct* 2022; 279: 114769.
21. Ryatt J and Ramulu M. Numerical investigation of the application of voxel based meshes for stochastic tow based discontinuous composites. *Finite Elem Anal Des* 2023; 214: 103874.
22. Pimenta S and Robinson P. An analytical shear-lag model for composites with "brick-and-mortar" architecture considering non-linear matrix response and failure. *Compos Sci Technol* 2014; 104: 111–124.
23. Czél G, Jalalvand M and Wisnom MR. Demonstration of pseudo-ductility in unidirectional hybrid composites made of discontinuous carbon/epoxy and continuous glass/epoxy plies. *Compos Part A Appl Sci Manuf* 2015; 72: 75–84.
24. Henry J and Pimenta S. Semi-analytical simulation of aligned discontinuous composites. *Compos Sci Technol* 2017; 144: 230–244.
25. Shi Y, Gillet A, Mantaux O, et al. Influence of the architecture on the strength of a unidirectional composite with recycled discontinuous fibres. *J Compos Mater* 2023; 57: 4169–4181.
26. Goutianos S, Cabrera NO, Alcock B, et al. Self-reinforced polypropylene composites based on discontinuous Tapes - an experimental and numerical study of the influence of tape length. *Appl Compos Mater* 2020; 27: 1–27.
27. Zweben C and Rosen BW. A statistical theory of material strength with application to composite materials. *J Mech Phys Solids* 1970; 1: 324.
28. Finley JM, Henry J, Shaffer MSP, et al. The influence of variability and defects on the mechanical performance of tailorable composites. *J Compos Mater* 2020; 54: 565–589.

29. Henry JJ. *Designing and modelling bio-inspired discontinuous composites*. Imperial College London: PhD Thesis, 2018.
30. Carvelli V, D'Ettorre A and Lomov SV. Acoustic emission and damage mode correlation in textile reinforced PPS composites. *Compos Struct* 2017; 163: 399–409.
31. Moffat AJ, Wright P, Buffière JY, et al. Micromechanisms of damage in 0° splits in a [90/0]s composite material using synchrotron radiation computed tomography. *Scr Mater* 2008; 59: 1043–1046.
32. Garcea SC, Mavrogordato MN, Scott AE, et al. Fatigue micromechanism characterisation in carbon fibre reinforced polymers using synchrotron radiation computed tomography. *Compos Sci Technol* 2014; 99: 23–30.
33. Mehdikhani M, Breite C, Swolfs Y, et al. Digital volume correlation for meso/micro in-situ damage analysis in carbon fiber reinforced composites. *Compos Sci Technol* 2021; 213: 108944.
34. Fotouhi M, Suwarta P, Jalalvand M, et al. Detection of fibre fracture and ply fragmentation in thin-ply UD carbon/glass hybrid laminates using acoustic emission. *Compos Part A Appl Sci Manuf* 2016; 86: 66–76.
35. Ramirez-Jimenez CR, Papadakis N, Reynolds N, et al. Identification of failure modes in glass/polypropylene composites by means of the primary frequency content of the acoustic emission event. *Compos Sci Technol* 2004; 64: 1819–1827.
36. Gutkin R, Green CJ, Vangrattanachai S, et al. On acoustic emission for failure investigation in CFRP: pattern recognition and peak frequency analyses. *Mech Syst Signal Process* 2011; 25: 1393–1407.
37. Li L, Lomov SV, Yan X, et al. Cluster analysis of acoustic emission signals for 2D and 3D woven glass/epoxy composites. *Compos Struct* 2014; 116: 286–299.
38. Ichenihi A, Li W and Gao Y. Damage analysis of combined continuous and discontinuous thin-ply carbon/glass hybrid composite using acoustic emission. *Polym Compos* 2021; 42: 6764–6776.
39. Czigány T, Marosfalvi J and Karger-Kocsis J. An acoustic emission study of the temperature-dependent fracture behavior of polypropylene composites reinforced by continuous and discontinuous fiber mats. *Compos Sci Technol* 2000; 60: 1203.
40. Lifton JJ, Malcolm AA, Mcbride JW, et al. The application of voxel size correction in X-ray computed tomography for dimensional Metrology. *Singapore International NDT Conference & Exhibition*. Singapore, July 19-20 2013.
41. Wagner HD. Stochastic concepts in the study of size effects in the mechanical strength of highly oriented polymeric materials. *J Polym Sci B Polym Phys* 1989; 27: 115–149.
42. Hashin Z. Failure criteria for unidirectional fiber composites. *J Appl Mech* 1980; 47: 329–334.
43. Hashin Z and Rotem A. A fatigue failure criterion for fiber reinforced materials. *J Compos Mater* 1973; 7: 448–464.
44. Sørensen BF, Goutianos S and Jacobsen TK. Strength scaling of adhesive joints in polymer-matrix composites. *Int J Solid Struct*. 2009; 46: 741–761.
45. Ganesh R and Gillespie JW. Dynamic 3D effects of single fiber tensile break within unidirectional composites including resin plasticity, residual stress, interfacial debonding and sliding friction. *J Compos Mater* 2023; 57: 4083–4102.

46. Ganesh R, Sockalingam S and Gillespie JW. Dynamic effects of a single fiber break in unidirectional glass fiber-reinforced polymer composites: effects of matrix plasticity. *J Compos Mater* 2018; 52: 1873–1886.
47. Kravchenko SG, Sommer DE and Pipes RB. Uniaxial strength of a composite array of overlaid and aligned prepreg platelets. *Compos Part A Appl Sci Manuf* 2018; 109: 31–47.
48. Airoldi A, Sala G and Bettini P. Evaluation of numerical approaches for the development of interlaminar damage in composite laminates. In: International Conference on Composite Materials, Kyoto, Japan July 8-13, 2007.
49. de Borst R, Crisfield MA, Remmers JJC, et al. Solution Techniques in Quasi-Static Analysis. *Non-Linear Finite Element Analysis of Solids and Structures, Second Edition*. 2012.
50. Bessell T and Shortall JB. The crystallization and interfacial bond strength of nylon 6 at carbon and glass fibre surfaces. *J Mater Sci* 1975; 10: 2035–2043.
51. Schmidt J, Klingenhöfer M, Kaufmann J, et al. Characterization of the interlaminar fracture toughness of unidirectional thermoplastic composites. *Technologies for Lightweight Structures (TLS)* 2022; 5: 77–85.
52. Turon A, Dávila C, Camanho PP, et al. An engineering solution for mesh size effects in the simulation of delamination using cohesive zone models. *Eng Fract Mech* 2007; 74: 1665–1682.
53. ABAQUS. *Analysis user's manual, version 6.14*. Dassault Systemes Simulia, Inc., 2014.
54. van den Heuvel PWJ, Goutianos S, Young RJ, et al. Failure phenomena in fibre-reinforced composites. Part 6: a finite element study of stress concentrations in unidirectional carbon fibre-reinforced epoxy composites. *Compos Sci Technol* 2004; 64: 645–656.
55. Curto M, Dowsett J, Kao AP, et al. Multi-material 3D printed composites inspired by nacre: a hard/soft mechanical interplay. *Sci Rep* 2025; 15: 6728.
56. Saeedifar M, Fotouhi M, Ahmadi Najafabadi M, et al. Prediction of quasi-static delamination onset and growth in laminated composites by acoustic emission. *Compos B Eng* 2016; 85: 113–122.
57. Saeedifar M and Zarouchas D. Damage characterization of laminated composites using acoustic emission: a review. *Compos B Eng* 2020; 195: 108039.
58. Benmedakhene S, Kenane M and Benzeggagh ML. Initiation and growth of delamination in glass/epoxy composites subjected to static and dynamic loading by acoustic emission monitoring. *Compos Sci Technol* 1999; 59: 201–208.
59. de Groot PJ, Wijnen PAM and Janssen RBF. Real-time frequency determination of acoustic emission for different fracture mechanisms in carbon/epoxy composites. *Compos Sci Technol* 1995; 55: 405–412.
60. Scholey JJ, Wilcox PD, Wisnom MR, et al. Quantitative experimental measurements of matrix cracking and delamination using acoustic emission. *Compos Part A Appl Sci Manuf* 2010; 41: 612–623.
61. Barkoula N-M, Alcock B, Cabrera NO, et al. Fatigue properties of highly oriented polypropylene tapes and all-polypropylene composites. *Polym Polym Compos* 2011; 132: 277.
62. Pimenta S and Pinho ST. The influence of micromechanical properties and reinforcement architecture on the mechanical response of recycled composites. *Compos Part A Appl Sci Manuf* 2014; 56: 213–225.

63. Thomason JL and Vlug MA. Influence of fibre length and concentration on the properties of glass fibre-reinforced polypropylene: 1. *Tensile and flexural modulus* 1996; 21.
64. Ganesh R, Obaid AA and Gillespie JW. Experimental determination of bimodal strength distribution of S-glass fibers. *Compos B Eng* 2023; 254: 110559.

Appendix

Appendix A

To calculate the Weibull parameters, the strength data from of the single-tape tests were sorted, and the cumulative probability of failure, P_f, was calculated by normalizing and cumulatively summing the occurrences of each strength value. The data was divided into 20 equally spaced bins between the minimum and maximum strength values for detailed analysis. To estimate the Weibull parameters, we applied a double logarithmic transformation to the cumulative probabilities, $ln\left(ln\left(\frac{1}{1-P_f}\right)\right)$, and took the natural logarithm of the corresponding strength values, $ln\,(\sigma)$. Linear regression was performed on these transformed variables to determine the Weibull shape parameter, w, and scale parameter, σ_0. The Weibull modulus for the tape (18.96) is significantly higher than that reported for glass fibres, which has been reported as between two and 6,[63] indicating less scatter in strength values for the tape than the individual fibres, an expected result given that each tape consists of thousands of fibres. The length of the tapes in this study are significantly above the critical fibre length, indicating the validity of extrapolating Weibull values calculated from the stochastic tests to the tape lengths in this study.[64]